THE JOURNAL OF BIOLOGICAL CHEMISTRY VOL. 282, NO. 26, pp. 19029–19041, June 29, 2007

Insights into the Structural Basis of the GADD45β-mediated Inactivation of the JNK Kinase, MKK7/JNKK2*[S]

Received for publication, April 12, 2007 Published, JBC Papers in Press, May 7, 2007, DOI 10.1074/jbc.M703112200

Salvatore Papa[‡], Simona M. Monti[§], Rosa Maria Vitale[§], Concetta Bubici[‡1], Shanthi Jayawardena[‡], Kellean Alvarez[‡], Enrico De Smaele[‡2], Nina Dathan[§], Carlo Pedone[§], Menotti Ruvo[§3], and Guido Franzoso[‡4]

From [‡]The Ben May Institute for Cancer Research, University of Chicago, Chicago, Illinois 60637 and the [§]Istituto di Biostrutture e Bioimmagini, Consiglio Nazionale delle Ricerche, Via Mezzocannone 16, 80134 Napoli, Italy

NF-κB/Rel factors control programmed cell death (PCD), and this control is crucial to oncogenesis, cancer chemoresistance, and antagonism of tumor necrosis factor (TNF) α-induced killing. With TNFα, NF-κB-mediated protection involves suppression of the c-Jun-N-terminal kinase (JNK) cascade, and we have identified Gadd45β, a member of the Gadd45 family, as a pivotal effector of this activity of NF-κB. Inhibition of TNFα-induced JNK signaling by Gadd45β depends on direct targeting of the JNK kinase, MKK7/JNKK2. The mechanism by which Gadd45β blunts MKK7, however, is unknown. Here we show that Gadd45β is a structured protein with a predicted four-stranded β-sheet core, five α-helices, and two acidic loops. Association of Gadd45β with MKK7 involves a network of interactions mediated by its putative helices α3 and α4 and loops 1 and 2. Whereas α3 appears to primarily mediate docking to MKK7, loop 1 and α4-loop 2 seemingly afford kinase inactivation by engaging the ATP-binding site and causing conformational changes that impede catalytic function. These data provide a basis for Gadd45β-mediated blockade of MKK7, and ultimately, TNFα-induced PCD. They also have important implications for treatment of widespread diseases.

NF-κB/Rel transcription factors promote cell survival, and this activity of NF-κB counters programmed cell death (PCD)[5] elicited by the pro-inflammatory cytokine tumor necrosis factor (TNF) α (1, 2). This inhibition of TNFα-induced PCD by NF-κB is crucial for sustaining chronic inflammation and tumor progression (2, 3). NF-κB afforded protection also serves immunity, lymphopoiesis, and cancer chemoresistance (1, 4, 5). We and others have shown that, downstream of TNF-Rs, the NF-κB-mediated antagonism of PCD involves a suppression of the sustained activation of the c-Jun N-terminal kinase (JNK) cascade (6, 7). This is one of the major mitogen-activated protein kinase (MAPK) pathways, and like other such pathways, it transduces signals through phosphorylation of hierarchically ordered kinase modules to elicit an appropriate cellular response (8). Prolonged activation of JNK by TNFα was shown to elicit PCD by causing Itch-dependent proteolysis of the caspase-8 antagonist, c-FLIP$_L$, and cleavage of Bcl-2-like factor, Bid, into proapototic jBid (2, 9, 10). Thus, the biological outcome of the triggering of TNF-Rs is determined by a delicate balance between the opposing activities of the JNK and NF-κB pathways.

The inhibitory activity that NF-κB exerts on the JNK cascade involves an up-regulation of target genes (1), and we have identified Gadd45β, a member of the Gadd45 family of structurally related factors (11), as the product of one of such genes (6). Gadd45β is induced rapidly by TNFα through a mechanism that requires NF-κB, its ectopic expression blocks TNFα-elicited JNK activity and PCD in NF-κB null cells, and gene targeted- or antisense-mediated inactivation of endogenous *gadd45β* impairs the NF-κB-mediated control of JNK signaling and PCD downstream of TNF-Rs (2, 6, 11). The Gadd45β-afforded blockade of this signaling depends on a direct targeting and inactivation of the MAPKK, MKK7/JNKK2, a selective and essential inducer of JNK following exposure to TNFα (11). Indeed, the Gadd45β-MKK7 interaction is a crucial molecular link between the NF-κB and JNK pathways, and accordingly, a key checkpoint controlling cell fate downstream of TNF-Rs (2, 11). The relevance of this link is underscored by the ability of cell-permeable peptides selectively interfering with the Gadd45β-mediated suppression of MKK7 to hinder NF-κB afforded cytoprotection against TNFα-induced killing (11), and the ability of short hairpin RNAs knocking-down *MKK7* to halt this killing in NF-κB null cells (9). Knock-out studies confirmed the essential role that Gadd45β plays in blocking TNFα-induced PCD in certain tissues (2, 11). Other such studies in mice also uncovered a requirement for Gadd45β in skeleton morphogenesis, cell resistance to stress- and anticancer drugs-induced killing, and differentiation and function of T-helper 1 (T_H1) T cells (11–14).

In many instances, the biological activity of Gadd45 factors has been linked to regulation of protein kinases, such as MAPK

* This work was supported in part by National Institutes of Health R01 Grants CA84040 and CA098583. Both laboratories contributed equally to this work. The costs of publication of this article were defrayed in part by the payment of page charges. This article must therefore be hereby marked "*advertisement*" in accordance with 18 U.S.C. Section 1734 solely to indicate this fact.

[S] The on-line version of this article (available at http://www.jbc.org) contains "Materials and Methods" and Figs. S1–S6.

[1] Supported in part by a fellowship from the American-Italian Cancer Foundation.

[2] Current address: Dept. of Experimental Medicine and Pathology, University of Rome "La Sapienza," Viale Regina Elena 324, 00161 Rome, Italy.

[3] To whom correspondence may be addressed. Tel.: 39-081-2536644; Fax: 39-081-2534574; E-mail: menotti.ruvo@ unina.it.

[4] To whom correspondence may be addressed. Tel.: 773-834-0020; Fax: 773-702-3701; E-mail: gfranzos@midway.uchicago.edu.

[5] The abbreviations used are: PCD, programmed cell death; TNF, tumor necrosis factor; JNK, c-Jun N-terminal kinase; MAPK, mitogen-activated protein kinase; GST, glutathione *S*-transferase; eGFP, enhanced green fluorescent protein; PTD, protein transduction domain; 4-VP, 4-vinylpyridine; LC-MS, liquid chromatography-mass spectrometry; CD, circular dichroism; FL, full-length.

pathway kinases (15–17). We showed for instance that Gadd45β binds directly to MKK7, and that this binding is sufficient alone to cause inactivation of this kinase. As other Gadd45 family proteins, however, Gadd45β lacks enzymatic activity such as phosphatase activity (16, 17), and so, the basis for its ability to block MKK7 remains unknown. To understand this basis, here we used a combined structural and functional approach. Using this approach, we constructed a model predicting that Gadd45β is a structured protein, consisting essentially of a central four-stranded β-sheet core surrounded by five α-helices and two acidic loops. In this model, contact of Gadd45β with MKK7 involves an extensive network of interactions mediated by its α-helices α3 (Ile^{69}-Asn^{85}) and α4 (Met^{95}-Leu^{102}) and loops 1 and 2 (Ile^{61}-Asp^{68} and Gly^{103}-Leu^{117}, respectively). Indeed, we found that whereas α3 plays a key role in docking of Gadd45β to MKK7, the loop 1 and α4-loop 2 regions of Gadd45β are essential for kinase inactivation. These regions appear in fact to establish several bonds with residues in the catalytic pocket and the β3-helix C loop of MKK7, preventing access of the kinase to ATP and inducing conformational changes that stabilize this kinase in an inactive conformation. These data provide a mechanism for Gadd45β-mediated suppression of MKK7, and ultimately, of TNFα-induced PCD (2). Given the key role that inappropriate blockade of PCD by NF-κB plays in chronic inflammation and cancer (1, 4, 5), they also have potential implications for development of new treatments for these diseases.

EXPERIMENTAL PROCEDURES

Protein Purification and Binding Assays—Glutathione *S*-transferase (GST) proteins used Figs. 1–4 were purified from bacterial lysates using glutathione beads (Sigma) as detailed elsewhere (11). Purity was verified by Coomassie Blue staining (Figs. 3*E* and 4*C*). For binding assays, *in vitro* translated proteins (5 μl) were incubated with GST (10 μl) proteins for 20 min and then pulled down with glutathione beads as described previously (11). Prior to loading onto gels, beads were washed extensively in binding buffer (20 mM Tris·HCl, pH 7.4, 150 mM NaCl, 0.2% Triton X-100; Figs. 1, *B*, *D*, and *F*, and 2*B*). In Fig. 2*D* and supplementary Fig. S5B, higher stringency was achieved by performing GST precipitations using 0.4% Triton X-100, 5 μl of translated proteins, and 4 μl of GST-coupled beads.

Kinase Assays—MKK7 kinase assays were performed as detailed elsewhere (11). Briefly, active FLAG-MKK7 was immunoprecipitated with an anti-FLAG antibody (Sigma) from lysates of HEK-293 cells treated with human TNFα (2,000 units/ml; Peprotech) for 10 min and then subjected to *in vitro* kinase reaction for 20 min at 30 °C. Preincubation with recombinant GST or GST-Gadd45β proteins was for an additional 10 min (Figs. 3, *B* and *D*, and 4*B*).

Additional Methods—A detailed description of additional materials and methods, including cell treatments and death assays, plasmids, human (h)Gadd45β purification, native gel electrophoresis, gel filtration, LC-MS, circular dichroism (CD), limited proteolysis and alkylation analyses, and modeling can be found in the supplementary data.

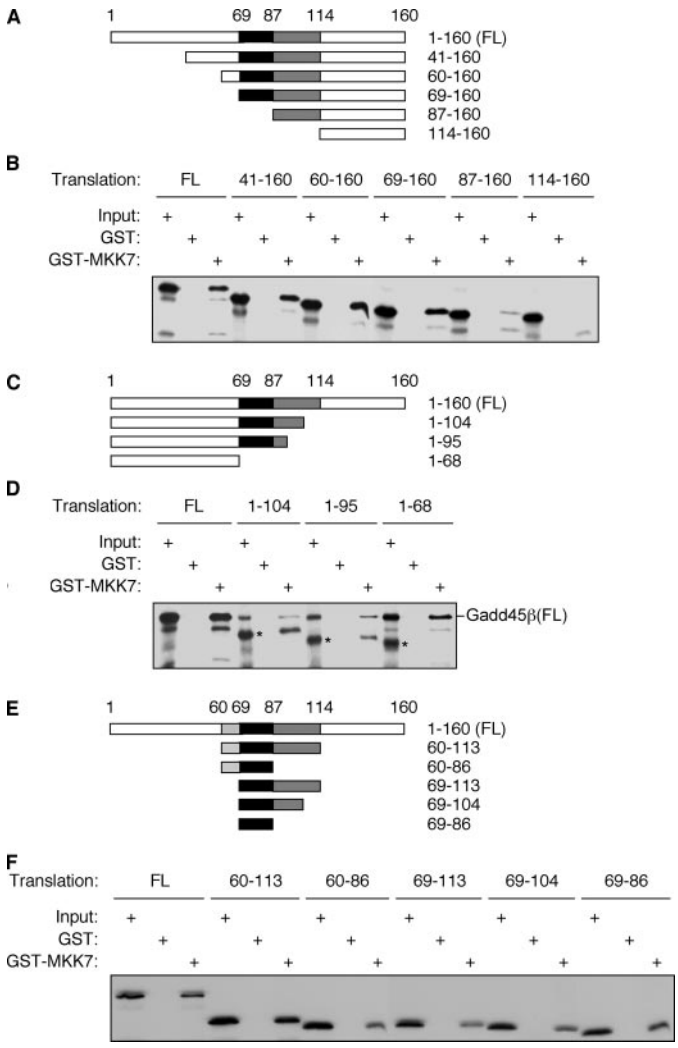

FIGURE 1. **Gadd45β interacts with MKK7 through an extended region comprising peptide 69–86.** *A*, *C*, and *E*, representation of the N- and C-terminal truncations and internal Gadd45β polypeptides used for binding assays, respectively. *Numbers* indicate amino acidic residues. Region 69–86 is shown in *black*; other MKK7-binding regions are in *gray*. *B*, *D*, and *F*, pull-down assays showing binding of GST- and GST-MKK7-coated beads to the ^{35}S-labeled, *in vitro* translated proteins depicted in *A*, *C*, and *E*, respectively. Shown is 40% of the inputs. *Asterisks* in *D* mark proteins synthesized from linearized pBS-Gadd45β(FL) templates. Full-length (FL) Gadd45β derived from undigested plasmids is also indicated.

RESULTS

Identification of the Regions of Gadd45β Contacting MKK7—Gadd45 proteins have no known enzymatic activity (16, 17). Thus, to determine the basis for Gadd45β-mediated inactivation of MKK7, we mapped the region(s) of Gadd45β involved in interaction with this kinase. Plasmids encoding N- or C-terminal truncated Gadd45β proteins were translated *in vitro* (Fig. 1, *A* and *C*, respectively), and the resulting products were tested for their ability to bind to GST-MKK7 fusion proteins in GST pull-down assays (Fig. 1, *B* and *D*). GST served as negative control. Full-length (FL) Gadd45β bound strongly to GST-MKK7, but not to GST (Fig. 1*B*), as shown previously (11). Gadd45β-(41–160), Gadd45β-(60–160), and Gadd45β-(69–160) also interacted with the fusion protein with high affinity (Fig. 1*B*; compare the fractions of precipitated products relative to their inputs), suggesting that residues 1–68 are dispensable for tight

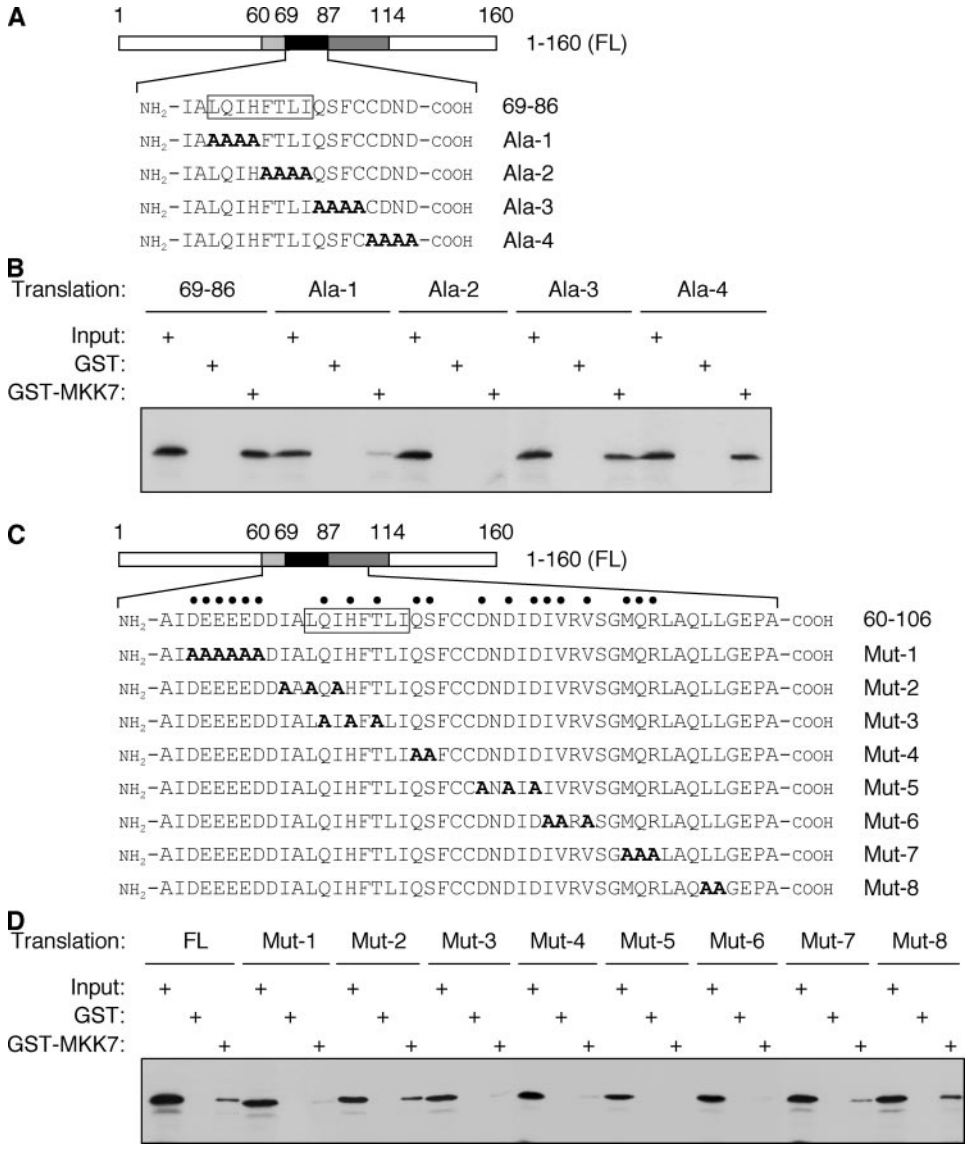

FIGURE 2. **Identification of Gadd45β residues mediating binding to MKK7.** *A* and *C*, representation of the Gadd45β-(69–87) and Gadd45β(FL) alanine-scanning mutants used for binding assays, respectively. MKK7-binding regions are in *black* or *gray*, with darkness correlating with the apparent relevance to this binding. Mutagenized residues are shown; alanine substitutions are *bold*. The Leu[71]–Ile[78] region is *boxed*; residues contributing to binding are *dotted*. *B* and *D*, pull-down assays showing binding of GST- or GST-MKK7-coated beads to the ^{35}S-labeled, *in vitro* translated products depicted in *A* and *C*, respectively. Shown is 40% of the inputs. In *B* and *D* different stringency was used (see "Experimental Procedures").

binding of Gadd45β to MKK7. Notably, removal of an additional 18 amino acids severely compromised this binding (Fig. 1*B*, see *87–160*), whereas further truncations also involving residues Ile[87]–Glu[113] abolished it (Fig. 1*B*, see *114–160*). These data suggest that region Ile[69]–Asp[86] is essential for association of Gadd45β with MKK7 and that the adjacent region Ile[87]–Glu[113] also contributes to this association.

Analysis of C-terminal truncations confirmed the presence of a MKK7 interaction region between Gadd45β residues 69 and 95 (Fig. 1*D*, compare *1–95* and *1–68*). Full-length Gadd45β, yielded by incomplete restriction digestion of pBS-*Gadd45β* templates (Fig. 1*D*), served as internal positive control. Together, these findings suggest that Gadd45β interacts with MKK7 primarily through region Ile[69]–Asp[86], and that additional contacts are made through Ile[87]–Glu[113].

These data do not exclude existence of additional MKK7-binding regions within Gadd45β (discussed below). The importance of the Ile[69]–Asp[86] region for this binding, however, was corroborated by findings with internal Gadd45β peptides (Fig. 1*E*). As shown in Fig. 1*F*, Gadd45β-(60–113) interacted with GST-MKK7 with high affinity (comparable with that of FL), and Gadd45β-(69–86) virtually recapitulated this interaction, suggesting that Ile[69]–Asp[86] is sufficient alone for tight association of Gadd45β with MKK7 (compare 69–86 to FL).

Delineation of Residues Involved in Interaction of Gadd45β with MKK7—To further delineate which residues of Gadd45β are most critical for binding to MKK7, we generated alanine-scanning mutants of region Ile[69]–Asp[86] (Fig. 2*A*). As shown in Fig. 2*B*, mutation of residues Leu[71]–His[74] or Phe[75]–Ile[78] (Ala-1 and Ala-2, respectively) severely compromised association of Gadd45β-(69–86) with MKK7, whereas mutation of residues Gln[79]–Cys[82] or Cys[83]–Asp[86] impacted on this association only modestly (Fig. 2*B*, Ala-3 and Ala-4, respectively), suggesting that contact with MKK7 is primarily mediated through the Leu[71]–Ile[78] segment of region Ile[69]–Asp[86].

Next, we introduced select mutations within the broader region Ala[60]–Ala[106] in the context of Gadd45β(FL) (Fig. 2*C*), because additional residues within this region appeared to be involved in association with MKK7 (discussed above; *see* Fig. 1). As shown in Fig. 2*D*, alanine substitutions of acidic residues Asp[62]–Asp[67] (Mut-1) significantly weakened Gadd45β interaction with MKK7 (compare with FL). Conversely, mutation of Ile[69], Leu[71], and Ile[73] (Mut-2) had no effect on this interaction, suggesting that the binding impairment seen with Ala[1] (Fig. 2*B*) was due to ablation of Gln[72] and/or His[74], and not of Leu[71] or Ile[73]. Indeed, substitution of the former residues, along with that of Thr[76] severely compromised Gadd45β association with MKK7 (Fig. 2*D*, *Mut-3*). Binding was also impaired by mutation of Asp[84]/Asp[86]/Asp[88] (Mut-5) or Ile[89]/Val[90]/Val[92] (Mut-6), and to a lesser extent, of Gln[79]/Ser[80] (Mut-4) or Met[95]/Gln[96]/Arg[97] (Mut-7) (Fig. 2*D*). Mut-8 precipitated with GST-MKK7 with efficiency comparable with that of Gadd45β(FL).

Notably, consistent with the notion that Gadd45β contacts MKK7 through an extended surface, beyond that created by

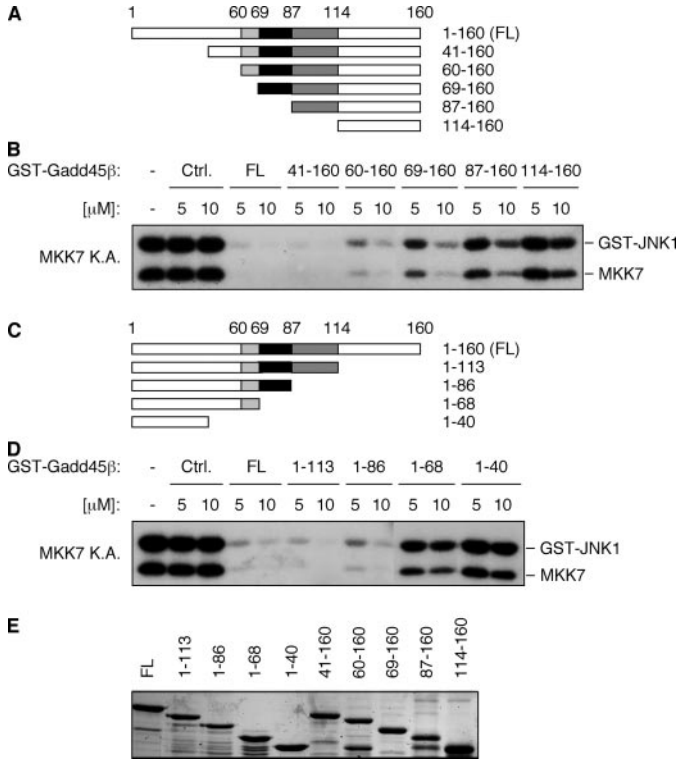

FIGURE 3. **Inactivation of MKK7 involves distinct regions of Gadd45β.** *A* and *C*, representation of the N- and C-terminal truncations of Gadd45β used for kinase assays, respectively. *Numbers* indicate amino acidic residues of the Gadd45β truncations used. MKK7-binding regions are colored as in Fig. 2*A*. *B* and *D*, kinase assays (*K. A.*) showing inhibition of active MKK7 by the indicated N- and C-terminal truncated GST-Gadd45β polypeptides. Immunoprecipitated MMK7, GST-JNK1 substrate, and concentrations of GST (*Ctrl.*) and GST-Gadd45β proteins are shown. (−), no inhibitor; (*FL*), GST-Gadd45β(FL). *E*, Coomassie Brilliant Blue staining showing purity of the proteins used in *B* and *D*.

Ile^{69}–Asp^{86}, alanine substitutions within Gadd45β(FL) had only partial inhibitory effects on the interaction of these proteins (Fig. 2*D* and data not shown), whereas the inhibitory effects of mutations introduced in the context of Gadd45β-(69–86) were virtually complete (Fig. 2*B*, Ala-2, and Ala-1). It is also noteworthy that, with the former mutants, binding assays were performed at higher stringency (see "Experimental Procedures"), which may explain in part why ablation of certain residues appeared to have more dramatic effects in the context of Gadd45β(FL) than in that of Gadd45β-(69–86) (*e.g.* see mutation of Gln^{79}/Ser^{80}; note binding of Mut-4 (Fig. 2*D*) and Ala-3 (Fig. 2*B*); see also Mut-5 (Fig. 2*D*) and Ala-4 (Fig. 2*B*), both containing mutations of Asp^{84}/Asp^{86}). It is also possible, however, that certain mutations had conformational effects that could be revealed only in the context of a full-length polypeptide (further discussed below; see also "Discussion"). In summary, the data suggest that binding of Gadd45β to MKK7 primarily involves Gln^{72} and/or His^{74}, as well as residues within peptide Phe^{75}–Ile^{78} such as Thr^{76}. They also suggest an involvement in this binding (either in direct contact with MKK7 or in maintenance of Gadd45β conformational stability) of additional residues both within and outside region Ile^{69}–Asp^{86} (*i.e.* Gln^{79}, Ser^{80}, Asp^{84} and/or Asp^{86}, within; and Asp^{62}–Asp^{67}, Asp^{88}, Ile^{89}, Val^{90}, Val^{92}, Met^{95}, Gln^{96}, and/or Arg^{97}, outside).

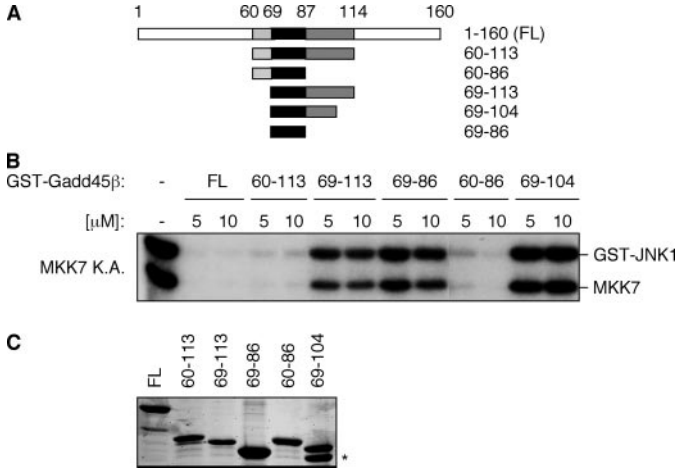

FIGURE 4. **Gadd45β regions 60–68 and 87–113 contain MKK7 inhibitory modules.** *A*, representation of the internal Gadd45β fragments used for kinase assays. *Numbers* and *black*/*gray* colors are used as in Fig. 3. *B*, kinase assays (*K. A.*) showing inhibition of active MKK7 by the indicated GST-Gadd45β proteins. Immunoprecipitated MMK7, GST-JNK1 substrate, and GST-Gadd45β protein concentrations are shown. (−), no inhibitor; (*FL*), GST-Gadd45β(FL); *asterisk*, truncated product. *C*, Coomassie Brilliant Blue staining showing purity of the proteins used in *B*.

Regions of Gadd45β Mediating MKK7 Inactivation—To delineate regions of Gadd45β involved in inhibition of MKK7, we examined the activity of N- and C-terminal Gadd45β truncations in MKK7 kinase assays, *in vitro* (Fig. 3, *A* and *C*, respectively). Active FLAG-MKK7 was isolated from TNFα-treated 293 cells, and kinase assays were performed in the presence of purified GST-Gadd45β proteins or control GST (Fig. 3, *B* and *D*; see also Fig. 3*E*). As shown previously, phosphorylation of GST-JNK1 by MKK7, as well as autophosphorylation, were effectively blocked by Gadd45β(FL) but not by GST (Ctrl), in a dose-dependent manner (Fig. 3, *B* and *D*; see also Ref. 11). The inhibitory activity of Gadd45β was virtually unaffected by removal of 40 N-terminal residues, and was affected only marginally by removal of an additional 19 amino acids (Fig. 3*B*, *41–160* and *60–160*, respectively), suggesting that region 1–59 is dispensable for effective blockade of MKK7 by Gadd45β. Notably, larger deletions progressively hindered the ability of Gadd45β to inhibit kinase function, with Gadd45β-(114–160) proteins virtually lacking any such ability (Fig. 3*B*). Gadd45β-(69–160) and, albeit to a lesser extent, Gadd45β-(87–160) retained instead significant inhibitory activity *in vitro*, but only at high concentrations.

Findings were confirmed by analysis of C-terminal Gadd45β truncations (Fig. 3, *C* and *D*). Deletion of residues 114–160 had no effect on Gadd45β afforded blockade of MKK7 (Fig. 3*D*, *1–113*), and a further deletion of residues 87–160 impacted upon this blockade only modestly, albeit reproducibly (Fig. 3*D*, *1–86*; see 5 μM). In contrast, a Gadd45β-(1–68) protein exhibited only weak inhibitory activity, and Gadd45β-(1–40) had virtually no such activity (Fig. 3*D*). These findings correlate with the physical interaction data shown in Fig. 1*B*, and suggest that Gadd45β-mediated inactivation of MKK7 involves, in addition to the MKK7-binding peptide Ile^{69}–Asp^{86} (Fig. 1*F*), two regions spanning Tyr^{41}–Asp^{68} and Ile^{87}–Glu^{113}.

To further delineate the role of these regions in inhibition of MKK7 and determine whether these are also sufficient for this

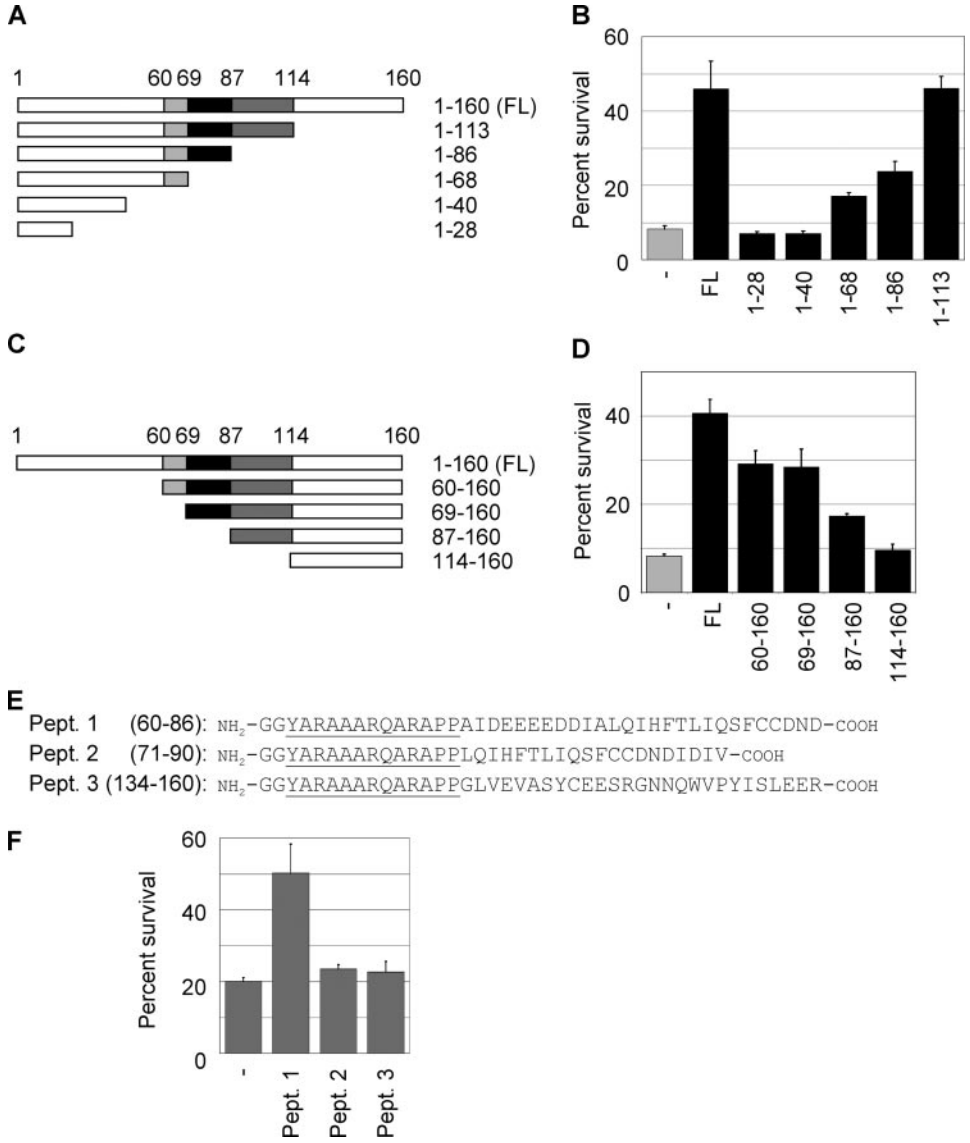

FIGURE 5. **Gadd45β-afforded protection involves the same regions that mediate inhibition of MKK7.** *A* and *C*, representation of the N- and C-terminal Gadd45β truncations used in cytoprotection assays, respectively. *Numbers* and *black/gray* colors are used as in Fig. 3. *B* and *D*, PI nuclear staining assays showing survival of *RelA*$^{-/-}$ cells expressing the indicated C- and N-terminal truncated Gadd45β proteins fused to eGFP, respectively, following treatment with TNFα plus low doses of cycloheximide (0.1 μg/ml). Percent survival reflects the fraction of live cells (*i.e.* DNA content ≥ G_1) in TNFα-treated cultures relative to control cultures treated with cycloheximide alone. (−), pEGFP; (*FL*), pEGFP-Gadd45β(FL). *E*, sequences of the PTD4 fusion peptides of Gadd45β used in *F*. PTD4 and the PP linker are *underlined*. *Numbers* designate the Gadd45β fragments fused to PDT4. *F*, viability of *RelA*$^{-/-}$ cells exposed to the indicated PTD4 fusion peptides or Me_2SO (−) and treated with TNFα plus 0.1 μg/ml cycloheximide. Percent survival reflects the fraction of live (*i.e.* adherent) cells in TNFα-treated cultures relative to control cultures treated with cycloheximide alone. Values in *B*, *D*, and *F* represent the mean (±S.D.) of three experiments. Intracellular peptide incorporation was verified through flow cytometry and confocal microscopy.

activity, we examined internal Gadd45β fragments (Fig. 4, *A*, see also *C*). As shown in Fig. 4*B*, Gadd45β-(60–86) exhibited strong inhibitory activity *in vitro*, even though at lower concentrations (*i.e.* 5 μM) this activity was somewhat weaker than that of Gadd45β(FL). Of interest, removal of the acidic stretch at Asp^{62}–Asp^{68} completely abolished kinase inactivation (Fig. 4*B*, compare *69–86* and *60–86*), suggesting that this stretch is crucial for inhibitory function. Notably, however, its relevance to this function was markedly less apparent in the context of longer Gadd45β polypeptides, extending C-terminal to either Glu^{113} or Arg^{160}. Indeed, these polypeptides, but not those extending only to Glu^{104}, were capable of affording significant suppression of MKK7 even in the absence of the Asp^{62}–Asp^{68} stretch (Fig. 4*B*, compare *69–86*, *69–104*, and *69–113*; see also Fig. 3*B*, note the inhibitory activity of *69–160*). These data are consistent with those shown in Fig. 3 and further support existence of a second MKK7 inhibitory module within Pro^{105}–Glu^{113}. Activity of this module was especially evident at lower protein concentrations (*i.e.* 5 μM or lower; *see* Figs. 3*B* and 4*B*; data not shown), suggesting that this plays an important physiologic role.

Altogether, the data indicate that high affinity binding of Gadd45β to MKK7 is mediated through region Ile^{69}–Asp^{86}, being both necessary and sufficient for this binding (Fig. 1). Association of Ile^{69}–Asp^{86} with MKK7, however, is insufficient alone to inhibit kinase activity (Fig. 4*B*). The suppressive action of Gadd45β on MKK7 depends in fact on establishment of further contacts involving the two inhibitory modules at Ala^{60}–Asp^{68} and Glu^{104}–Glu^{113}.

Gadd45β Regions Mediating Suppression of TNFα-induced PCD—To tighten the link between Gadd45β-mediated suppression of MKK7 and antagonism of TNFα-induced PCD (2), we examined whether these activities of Gadd45β were mediated by the same peptidic regions. To this end, C- and N-terminal truncations of Gadd45β (Fig. 5, *A* and *C*, respectively) were tested in cytoprotection assays in *RelA*$^{-/-}$ cells. As shown previously (6), upon expression of a fusion protein of enhanced green fluorescent protein (eGFP) and Gadd45β(FL), these cells were effectively rescued from TNFα-induced killing, with more than 50% of eGFP-Gadd45β(FL)-expressing cells being viable at 12.5 h (Fig. 5*B*). Cells expressing eGFP(−) remained susceptible to this killing, as expected. Deletion of residues 114–160 had no apparent effect on the ability of Gadd45β to counter TNFα-induced PCD (Fig. 5*B*, *1–113*), whereas larger deletions progressively impaired this ability, with a Gadd45β protein spanning residues 1–40 completely lacking such ability (Fig. 5*B*, *1–40*, also *1–28*). Hence, as for inhibition of MKK7, *in vitro* (Figs. 3 and 4), Gadd45β depends for antiapoptotic function on a peptidic segment comprised between Tyr^{41} and Asp^{113}.

Consistent with this notion, removal of residues 1–113 abolished the ability of Gadd45β to blunt TNFα-induced PCD, whereas a Gadd45β-(87–160) protein retained weak, but significant protective activity (Fig. 5*D*, *114–160* and *87–160*, respectively). Deletion of residues 1–68 yielded a protein that could effectively counter TNFα cytotoxicity, but was significantly less effective than Gadd45β(FL) in this action (Fig. 5*D*, compare *69–160* and *FL*). These data are consistent with the presence of a critical protective module within Ile^{69}–Glu^{113}, a region also required for inhibition of MKK7 (Figs. 3 and 4). They also suggest the existence of a second protective module within Met^{1}–Asp^{68}, a region harboring the Asp^{62}–Asp^{68} peptide, also involved in MKK7 inactivation (Fig. 4*B*).

Surprisingly, however, removal of residues 1–59, which do not contain this Asp^{62}–Asp^{68} peptide, impacted on the ability of Gadd45β to counter TNFα-elicited PCD to an extent similar to that of deletion of region 1–68 (Fig. 5*D*, see *60–160* and *69–160*). To clarify the involvement of Asp^{62}–Asp^{68} in cytoprotection, we therefore tested the activity of a synthetic protein transduction domain (PTD) 4-Gadd45β-(60–86) peptide in $RelA^{-/-}$ cells. This peptide consisted of region Asp^{62}–Asp^{68} and the MKK7-binding region, Ile^{69}–Asp^{86}, fused to a PTD4 peptide (Fig. 5*E*, peptide 1), which enables transduction through biological membranes (18). As shown in Fig. 5*F*, exposure to peptide 1, but not to control peptides 2 or 3 (71–90 and 134–160), which fail to block MKK7 *in vitro* (Figs. 1*F* and 4*B*; data not shown), effectively rescued $RelA^{-/-}$ cells from TNFα-induced PCD. Me_2SO-treated cells remained susceptible to this PCD, as expected (Fig. 5*B*). Peptides entered cells with comparable efficiency, shown by flow cytometry and confocal microscopy (data not shown). These data indicate that the Asp^{62}–Asp^{68} module can afford significant protection against TNFα-inflicted killing, regardless of the presence of Ile^{87}–Glu^{113}.

We concluded that Gadd45β-mediated protection involves participation of two distinct peptidic regions at Ala^{60}–Asp^{68} and Ile^{87}–Asp^{113}. Activity of these regions is markedly increased by the presence of peptide Ile^{69}–Asp^{86}, containing a key MKK7-binding module (Figs. 1 and 2). Although they are capable of acting somewhat independently, regions Ala^{60}–Asp^{68} and Ile^{87}–Asp^{113} are likely to function cooperatively *in vivo* to maximize suppression of TNFα-induced PCD. Hence, the ability of Gadd45β to counter TNFα-induced PCD tightly correlates with its ability to block MKK7 (Figs. 1–4), further validating the view that these two activities of Gadd45β are inseparable from one another (2).

Characterization of the Structure of Gadd45β—To investigate the structure of Gadd45β, a recombinant protein of human (h)Gadd45β was purified from bacterial lysates, upon removal of the fused GST tag by PreScission protease (Amersham Biosciences). The isolated protein was ~98% pure and had an apparent molecular mass of 18,096.8 ± 0.5 Da (inclusive of the GPLGS linker left from proteolytic cleavage), as shown by LC-MS analyses (supplementary Fig. S1, data not shown). Further studies involving native gel electrophoresis and gel filtration chromatography established that, like Gadd45α (19), Gadd45β exists primarily as a dimer, assembled through non-covalent bonds.[6] Lack of inter- and intramolecular disulfide bonds was further confirmed through alkylation of cysteine residues with 4-vinylpyridine (4-VP) followed by LC-MS analysis of tryptic hGadd45β fragments (*see* below).

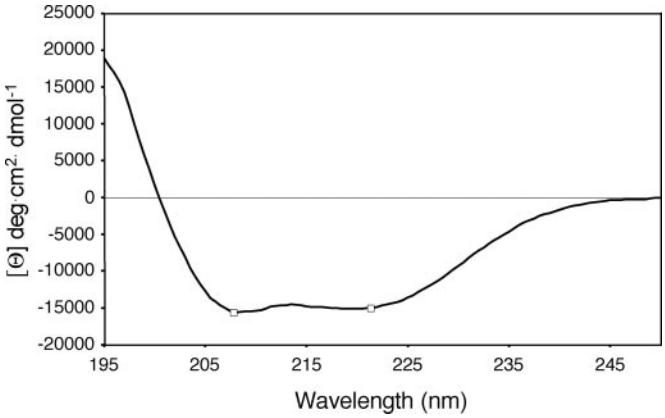

FIGURE 6. **CD spectrum of purified hGadd45β in the far UV region.** Shown is the profile of hGadd45β in the far UV region. The two negative peaks at 209 and 219 nm, indicative of high α-helical content, are indicated by *open squares*.

To assess the secondary structure of Gadd45β, we then used CD recording protein spectra in the far UV region (*i.e.* 195–250 nm). As shown in Fig. 6, the CD spectrum of native hGadd45β exhibited two negative peaks at 209 and 219 nm and one positive peak at 195 nm, indicative of a predominantly folded structure with a high α-helical content (*i.e.* ~45%) (20). This structure was also highly stable, because its CD spectrum was not significantly affected by exposure to either denaturing agents such as guanidinium hydrochloride (1 M) or structuring solvents such as trifluoroethanol (50% v/v) (data not shown).

To extend these studies, we then probed chain flexibility and accessibility of exposed residues to solvent by performing limited proteolysis assays, using several enzymes (21). Time progression analyses of trypsin digestion showed that the final proteolytic event occurred at Arg^{91}, with peaks produced by this event being recorded by LC-MS only at 720 min (supplementary Fig. S2A). This inaccessibility to trypsin suggested that this residue was either buried within the protein or contained within a non-flexible structure (see below; Fig. 7, *B* and *C*). Cleavages at Arg^{32}, Lys^{45}, Lys^{131}, and Arg^{146} also proceeded slowly, whereas cleavage at other sites occurred more readily (supplementary Fig. S2A), suggesting that unlike the former residues, the latter sites were exposed to the outer surface of the protein (see Fig. 7, *B* and *C*). Findings were extended by the use of α-chymotrypsin. As shown in supplementary Fig. S2B, kinetic analyses of the digested products revealed that hydrophobic residues Leu^{27}, Leu^{56}, and, to a lesser extent, Trp^{130} and Tyr^{141} were exposed to the enzyme. Chain flexibility at the N and C termini of Gadd45β was finally confirmed by the use of Glu-C. Digestion with this enzyme overall proceeded slowly, with complete cleavages being recorded at the N and C termini of the protein only after 10 h (supplementary Fig. S2C). The first of these cleavages occurred at Glu^{25}, followed by two other cleavages at Glu^{42} and Glu^{137}. The central core of the protein

[6] L. Tornatore and M. Ruvo, manuscript in preparation.

was unaffected by the enzyme, throughout the course of the reaction.

Next, we assessed accessibility of cysteine residues to solvent by performing limited thiol alkylation reactions using 4-VP and purified hGadd45β. As shown in supplementary Fig. S3A, following these reactions, ~90% of the protein harbored two molecules of 4-VP (18,310.4 ± 0.5 Da), whereas the remaining 10% incorporated three such molecules (18,416.3 ± 0.5 Da). Proteolysis with trypsin of these partially alkylated products followed by LC-MS analysis revealed that residue Cys^{9} (within Thr^{2}-Lys^{15}) and one of three cysteines within Leu^{46}–Arg^{91} (*i.e.* Cys^{57}, Cys^{82}, or Cys^{83}) were consistently alkylated in virtually all products (supplementary Fig. S3B). Conversely, fragment $Ser^{132–146}$, containing Cys^{142}, was alkylated only partially, because unmodified peptide was also detected readily (see supplementary Fig. S3B). To precisely delineate which cysteine within Leu^{46}–Arg^{91} was alkylated by 4-VP, we then used α-chymotrypsin. Combined LC-MS and MS/MS analyses of α-chymotrypsin-digested products revealed the presence of a monoalkylated Cys^{82}–Met^{95} peptide, which upon fragmentation, was found to be derivatized on Cys^{83}, establishing reactivity of this residue (data not shown). We concluded that, among the six cysteines of Gadd45β, accessibility to solvent was highest for Cys^{9} and Cys^{83}, followed by Cys^{142}. The other three cysteines were instead unreactive to 4-VP, suggesting that they were buried within the protein.

Modeling of Gadd45β—A search of the NCBI Conserved Domain Data Base using reverse position-specific BLAST and the FUGUE server (22, 23) identified Gadd45 proteins as members of the L7Ae/L30e/S12e family of structurally related, ribosomal polypeptides (24). Despite low sequence identity (<20%), Gadd45β exhibits a high degree of similarity in secondary structure profile with spliceosomal protein 15.5K (25), a member of this family, with gaps/insertions between these proteins being distributed preferentially in loop regions (Fig. 7*A*). The selection of 15.5K as template along with introduction of secondary structure restraints, based both on experimental data yielded by limited proteolysis and alkylation analyses (Fig. 6 and supplementary Figs. S2A–C and S3A-B, data not shown) and secondary structure predictions, enabled an accurate modeling of the structure of Gadd45β (Fig. 7*A*, further details can be found in the supplementary data, Materials and Methods section; see also Ref. 26).

The model indicates that hGadd45β is essentially constituted by a series of alternating α-helices and β-strands, which form a α-β-α sandwich-like structure (Fig. 7, *B* and *C*). This is characterized by a central four-stranded β-sheet core consisting of three antiparallel and one parallel β-strands, ordered as follows: Leu^{36}–Val^{38} (β1), His^{118}–Thr^{123} (β4), Val^{54}–Ala^{60} (β2), Asn^{88}–Val^{92} (β3). The five α-helices are oriented such that Gln^{17}–Gln^{33} (α1), Met^{95}–Leu^{102} (α4), and Lys^{131}–Arg^{146} (α5) lie on one side of the β-sheet, and Val^{40}–Val^{49} (α2) and Ile^{69}–Asn^{85} (α3) pack against the other. The main insertions relative to template are located in the acidic loops at Ile^{61}–Asp^{68} and Gly^{103}–Leu^{117} (loop 1 and 2, respectively). MD trajectory analysis of both human and mGadd45β further indicated that the fold of the protein is stabilized by several H-bonds and salt bridges between the side chains of the following charged/polar residues: Arg^{91} (β3) and Gln^{79} (α3), Arg^{146} (α5) and Asp^{86} (α3-β3 loop)/Asn^{88} (β3), Lys^{131} (α5) and Glu^{25} (α1), Arg^{97} (α4), and Gln^{17}/Glu^{24} (α1).

This model is fully consistent with the experimental data, including the limited proteolysis and alkylation data (Fig. 6 and supplementary Figs. S2A-C and S3A-B; data not shown). It shows in fact that the six cysteines of hGadd45β are too far apart from each other to engage in disulfide bridges, explaining why no such bridges are found in the pure protein.[6] It also explains the ready accessibility to alkylation of Cys^{9} and Cys^{83} (supplementary Fig. S3 and data not shown), which exhibit a solvent accessible surface of >40% (Fig. 7, *B* and *C*), as well as the modest reactivity of Cys^{142} (supplementary Fig. S3B and data not shown), exhibiting a solvent accessible surface value of ~3%. In further agreement with the data, the remaining three cysteines of Gadd45β appear to be buried instead within the protein (solvent accessible surface <3%), two lying within the β-sheet core and one within α3 (Fig. 7, *B* and *C*). Robustness of the model was further validated by the virtual inaccessibility to proteases of Arg^{91} (β3) (supplementary Fig. S2A-C), buried in fact within the protein, and the presence of Arg^{32}, Lys^{45}, Lys^{131}, and Arg^{146} within highly organized, α-helical structures (Fig. 7, *A–C*).

Modeling of MKK7—MKK7 is a member of the protein kinase family, the largest family of polypeptides folding into a topologically defined, two-lobe structure (27). The smaller, N-terminal lobe of these proteins essentially consists of a five-stranded β-sheet structure and a so-called helix C, and is involved in nucleotide anchoring and orientation (27, 28). The C-terminal lobe comprises instead a predominantly α-helical structure containing six major α-helices, three β-strands, and the catalytic and activation loops, and is primarily responsible for substrate binding and phosphotransfer initiation (Fig. 8 and supplementary Fig. S4). The deep cleft between the two lobes hosts the ATP binding site. Twelve residues within the kinase domain are nearly invariant throughout the protein kinase superfamily (supplementary Fig. S4), these residues being crucial for catalytic function (27, 28).

To model the kinase domain of MKK7 (Tyr^{113}-Met^{398}), we used as template the crystallographic structure of the corresponding domain of TAO2 (31.1% identity) (29), instead of that of MEK-1 (30), despite that this had a higher sequence identity with MKK7 (*i.e.* 39.4%). This is because the x-ray structure of MEK-1 was resolved in the presence of a non-competitive antagonist, which caused a peculiar deformation of the catalytic site (30). The sequence of MEK-1 was, nevertheless, utilized for multiple alignment with TAO2 and MKK7, to facilitate correct positioning of conserved residues during model building (supplementary Fig. S4). The backbone-atom best fit of the final model of MKK7 on the chosen template yielded a root mean square deviation value of 0.359 Å.

Expectedly, this model shows that the structure of the kinase domain of MKK7 is very similar to that of other such domains of MAPKs (Fig. 8; also supplementary Fig. S4) (27, 30). Indeed, in this model, the ATP-binding site of MKK7 is formed by a number of highly conserved residues (27, 30). The backbone amide of Thr^{130} appears to be involved in H bonds with oxygen atoms of the phosphate groups of ATP. Furthermore, Lys^{149},

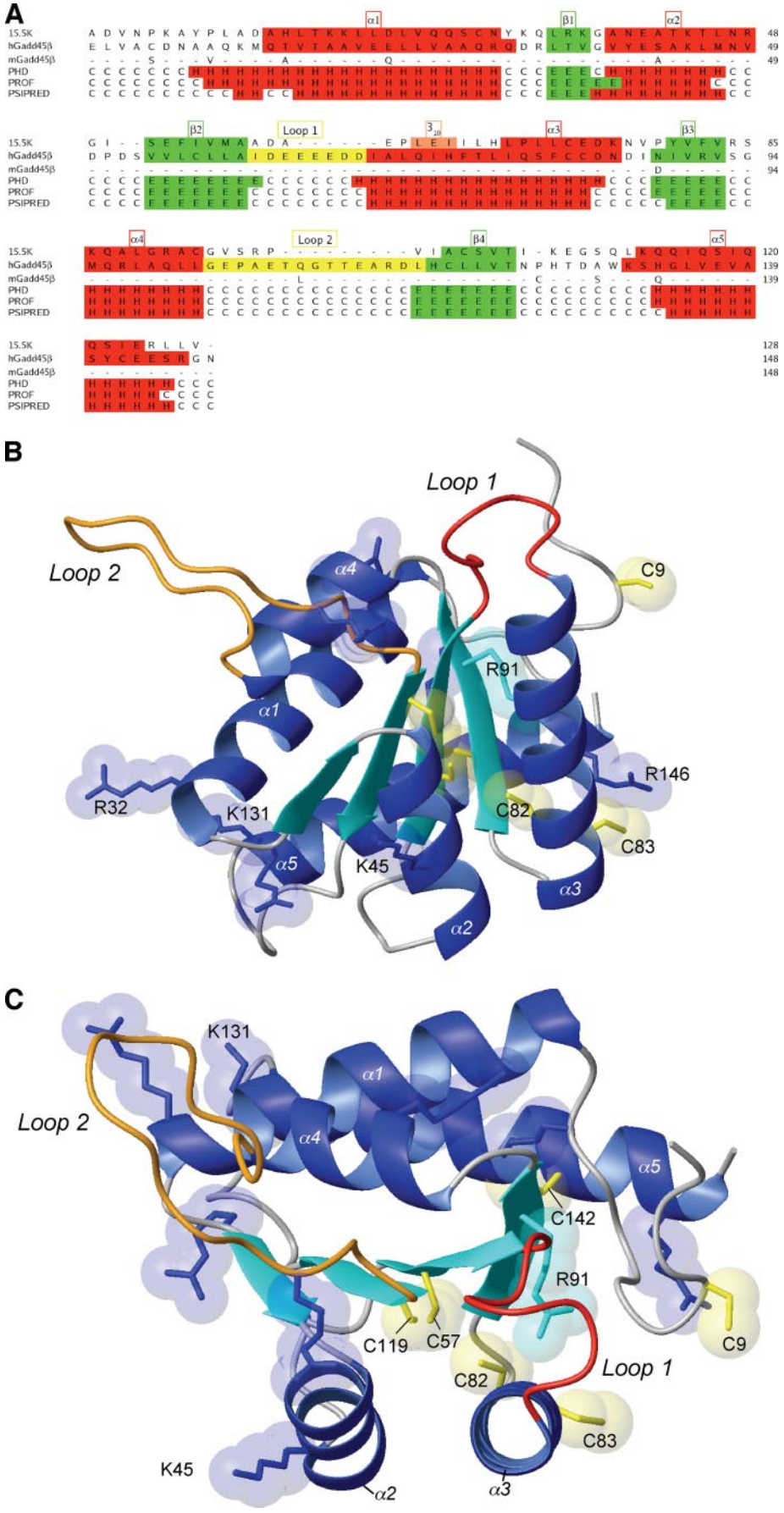

the invariant residue within β3, known to play a crucial role in anchorage and orientation of ATP in other protein kinases, contacts in the modeled MKK7 the three-phosphate group of the nucleotide (Fig. 8) and forms a salt bridge with the carboxyl group of the nearly invariant residue Asp[166]. In the model, Glu[197] and Met[199] too contribute to ATP anchorage by forming H bonds with the adenine ring of the nucleotide. Met[126], Val[134], Ala[147], Met[196], Leu[198], Met[199], and Leu[250] further participate in formation of the hydrophobic pocket that accommodates this ring.

Modeling of the MKK7-Gadd45β Complex—The modeled kinase domain of MKK7 appears to be positively charged, bearing a net value of +6 (supplementary Fig. S4). Mapping of the electrostatic potential onto the molecular surface showed a localized, positive patch at the interface between the N- and C-terminal lobes, in correspondence of the ATP-binding site (Fig. 8, data not shown). In contrast, Gadd45β is a highly negatively charged protein (net value of −16), and the largest acidic regions on its surface are those primarily formed by its N terminus and those modeled as loops 1 and 2 (Fig. 7, *A*–*C*, data not shown). Loop 1, in particular, is a stretch of all-negative residues that could potentially interact with residues of MKK7 involved in binding to the three-phosphate group of ATP (27, 30). This hypothesis is strongly supported by experimental evidence, because the basic residue-rich region 132–156 (comprising β2 and β3) was previously identified as a dominant Gadd45β-binding site of MKK7 (11). Indeed, screening of 2,000 different arrangements of the MKK7-Gadd45β complex generated with the ZDOCK program (31) confirmed preferential clustering of models exhibiting loop 1 in close proximity of the ATP-binding site of MKK7.

To further refine these models, we then took into account the finding that truncations of MKK7 spanning residues 63–401, 91–401, and

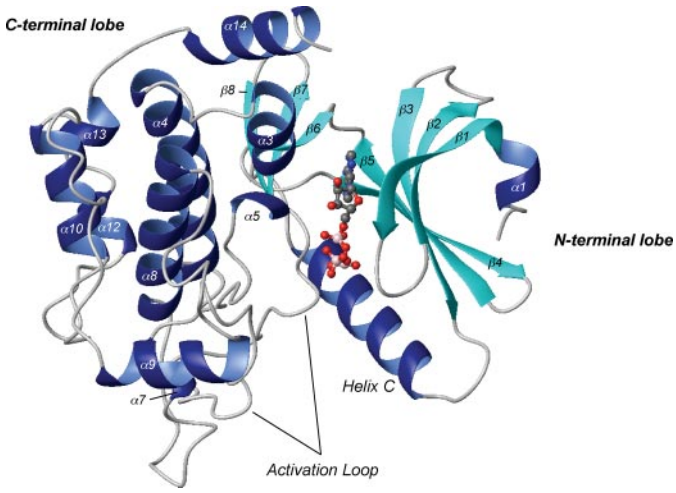

FIGURE 8. **Model of the kinase domain of MKK7 (Tyr^{113}—Met^{398}) bound to ATP, in ribbon representation.** ATP is in ball and stick representation. α-Helices are in *blue*, and β-strands are in *cyan*, as indicated.

132–401 bind to Gadd45β with affinity seemingly comparable with that of full-length MKK7 (11). We also accounted for the aforementioned crucial importance for this binding of β2–β3 of MKK7 (11). The dispensability of β1 for association of MKK7 with Gadd45β was instead likely due to the high relative content in acidic residues of this strand (supplementary Fig. S4). It is plausible, in fact, that to enable interaction of β2–β3 with Gadd45β and insertion of loop 1 into the catalytic cleft of MKK7, β1, may have to unfold, as seen in the interaction of cyclin-dependent kinase 2 with its inhibitor, p27^{KIP1} (Ref. 32, see "Discussion"). In light of these findings and considerations, we performed docking of Gadd45β onto a truncated MKK7 protein spanning residues 129–398, rather than onto a full-length kinase domain, as done previously with the cyclin-dependent kinase 2-p27^{KIP1} complex (32). We also removed 10 residues from the N terminus of Gadd45β, as these were both unstructured and dispensable for interaction with MKK7 (Figs. 7, *A–C*, and 1, respectively). The MD-refined complex that exhibited the lowest potential energy, strongest intermolecular H-bond interactions, and highest hydrophobic/hydrophilic complementarity, along with the lowest accessible surface for residues contacting ATP, is depicted in Fig. 9*B*.

Notably, this modeled complex fully accounts for the *in vitro* binding data, including the site-directed mutagenesis data (Figs. 1 and 2), as well as the functional data shown in Figs. 3 and 4 (see "Discussion"). Specifically, it suggests that Gln^{72} and Thr^{76} (α3) of Gadd45β are involved in H-bonds with Lys^{205} and Lys^{208} (α3) of MKK7, respectively (Fig. 9, *B* and *C*). It also suggests that Gln^{96} (α4) and Asp^{116} (loop 2) of Gadd45β interact with the guanidinium group of the side chain of Arg^{152} (β3) of MKK7, that Gln^{109} (loop 2) is H-bonded to MKK7 Arg^{153} (β3), and that Glu^{113} (also loop 2) is salt-bridged to the side chain of Lys^{157} (helix C-β3 loop) (Fig. 9*C*). Several contacts appear also to be made between loop 1 of Gadd45β and residues in the catalytic pocket of MKK7. Indeed, the model shows that Asp^{62} and Glu^{64} in this loop form H-bonds with the backbone amide groups of Gly^{129}, Thr^{130}, Cys^{131} (all within the β1–β2 loop), and Val^{134} (within β2) of MKK7, whereas Glu^{65} and Glu^{66} (also in loop 1) are salt-bridged to the side chains of MKK7 Lys^{149} (β3) and Arg^{162} (helix C), respectively (Fig. 9*C*). Finally, Met^{95} and Gln^{96} (α4) of Gadd45β are depicted to form van der Waals interactions with the side chains of Pro^{133} (β2) and Trp^{135} (β2) of MKK7, respectively (Fig. 9*C*).

To further validate the proposed model of the MKK7-Gadd45β complex, we tested its prediction that residues within putative Gadd45β acidic loops 1 and 2 (*i.e.* Glu^{65}, Glu^{66}, and Glu^{113}) directly contact basic residues within the catalytic pocket of MKK7 (*i.e.* Lys^{149}, Lys^{157}, and Arg^{162}). To this end, we performed GST pull-down assays using the "swapped" MKK7 and Gadd45β mutants depicted in supplementary Fig. S5A and S5B. As shown in supplementary Fig. S5B, the MKK7(K149E,K157E,R162E) and MKK7(K149E,R162E) mutants failed to bind to wild-type Gadd45β(FL) proteins (*lanes 3* and *12*, respectively), under conditions that enabled strong binding of these proteins to wild-type MKK7 (GST-MKK7) (see *lanes 2* and *11*). Remarkably, swapping mutations of cognate acidic residues of Gadd45β, predicted by our model to interact via salt bridges with the mutated basic amino acids of MKK7, partially restored binding of mutant MKK7 proteins to Gadd45β polypeptides (supplementary Fig. S5B; compare binding of Gadd45β (E65R,E66R,E113R) to wild-type and MKK7 (K149E,K157E,R162E) proteins (*lanes 3* and *9*, respectively); also compare binding of Gadd45β (E65R,E66R) to wild-type and MKK7 (K149E,R162E) proteins (*lanes 12* and *18*, respectively)). Rescue by these mutations was, nevertheless, incomplete, possibly due to conformational distortions caused by changes in the electrostatic charge of the targeted proteins. In contrast to what was seen with mutated MKK7 proteins, introduction of the aforementioned E65R,E66R,E113R and E65R,E66R mutations markedly impaired binding of wild-type MKK7 to Gadd45β polypeptides (supplementary Fig. S5B; compare *lanes 2* and *11* (FL) with *lanes 8* and *17* (E65R,E66R,E113R and E65R,E66R, respectively)). Somewhat expectedly, wild-type MKK7 retained weak binding activity for mutated Gadd45β polypeptides, likely owed to its preserved ability to form other interactions with these polypeptides (see Fig. 9). Under the conditions used, none of the tested MKK7 proteins exhibited significant association with Gadd45β(Mut-1) (supplementary Fig. S5B; *lanes 4–6* and *13–15*; see also Fig. 2*D*). Together, these data further validate our proposed model of the Gadd45β-MKK7 com-

FIGURE 7. *A*, sequence alignment of human and murine Gadd45β with 15.5 K. Observed (with 15.5K) and predicted (with Gadd45β; based on the PHD, PROF, and PSIPRED programs) secondary structure elements are highlighted: *red*, α-helix; *green*, β-strand; *orange*, 3_{10} helix. Loops 1 and 2 are in *yellow*. Highlighted residues in the sequence of hGadd45β take into account the revisions made in the final models depicted in *B* and *C*. The output of each secondary-structure prediction program used with hGadd45β (*i.e.* PHD, PROF, and PSIPRED) is shown. *H*, α-helix; *E*, β-strand; *C*, random coil. *B* and *C*, different views of the three-dimensional model of hGadd45β in ribbon representation. Loops 1 and 2 are shown in *red* and *orange*, respectively; α-helices, *blue*; β-strands, *cyan*. Arg and Lys residues that were experimentally shown to be exposed to solvent are depicted as *blue* stick bonds and transparent van der Waals surfaces. Arg^{91} (shown to be buried within the protein) is in *cyan*. Cys residues are in *yellow*.

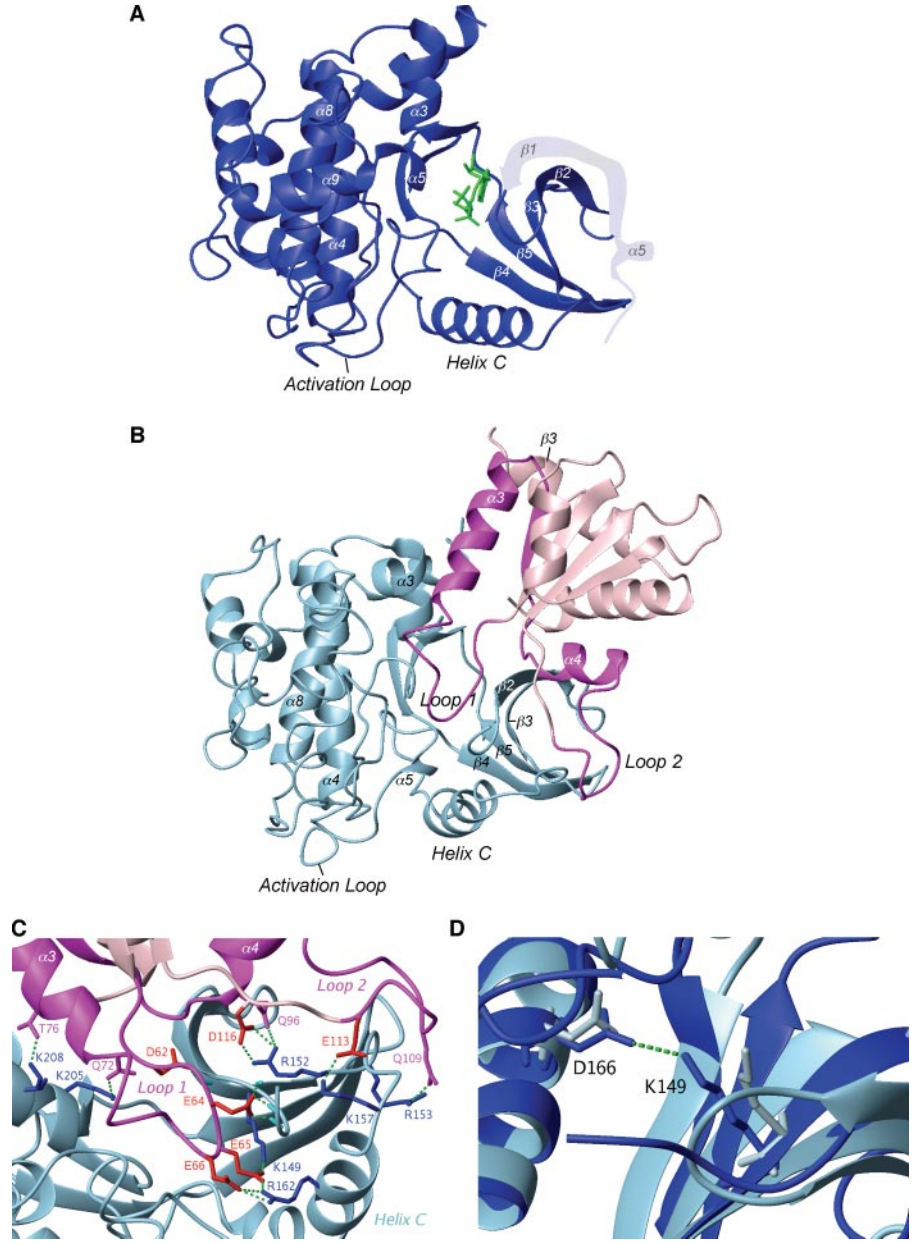

FIGURE 9. *A*, model of the kinase domain of MKK7 in ribbon representation and complexed to ATP, depicted as *green* bond sticks. MKK7 is shown in *blue*, with β1 (Tyr^{113}-Ser^{128}) (not included in the model) being transparent. *B*, model of the Gadd45β-MKK7 complex following MD simulation in ribbon representation, and *C*, details of the MKK7-Gadd45β interaction. MKK7 is in *light blue*; Gadd45β is in *pink*, with the 60–114 region shown in *magenta*. In *C*, polar residues involved in intermolecular side chain-side chain interactions at the MKK7-Gadd45β interface are in bond stick representation. Among these, acidic residues of Gadd45β are in *red*; basic residues of MKK7 are in *blue*. Other polar residues are colored according to their ribbon. H-bonds are depicted as *green dotted lines*. *D*, details of the interaction between the side chains of Lys^{149} and Asp^{166}, shown in stick representation and colored according to their ribbon. Shown are the models of MKK7, prior to (*i.e.* in active conformation; *blue*) and after (*i.e.* in the Gadd45β-bound, inactive conformation; *light blue*) MD simulation, superimposed at the backbone atoms level. The H-bond between Asp^{166} and Lys^{149} in the active kinase is shown in *green*.

plex and underscore the importance of the predicted salt bridges between residues Lys^{149}, Lys^{157}, and Arg^{162} of MKK7 and glutamic residues of putative loops 1 and 2 of Gadd45β in formation of this complex.

In summary, the model suggests that Gadd45β establishes an extensive network of interactions with MKK7: the first two turns of Gadd45β α3 interact with α3 of MKK7, thereby enabling insertion of loop 1 into the catalytic cleft; loop 2 of Gadd45β interacts instead with β3 and the two loops of MKK7 linking β3 to helix C and β4 to β5 (Fig. 9*B*). This model is strongly supported by experimental data and provides a mechanism for Gadd45β-mediated blockade of MKK7.

DISCUSSION

Here, we propose a mechanism for the Gadd45β-mediated suppression of MKK7, and ultimately, of TNFα-induced PCD (Fig. 5). Gadd45β is a structured protein, predicted to have a four-stranded β-sheet core surrounded by five α-helices and two acidic loops, a prediction fully consistent with CD, limited proteolysis, and alkylation studies (Figs. 6 and 7; supplementary Figs. S2 and S3; data not shown). Furthermore, site-directed mutagenesis data and the presented optimized model of the MKK7-Gadd45β complex suggest that this protein associates with MKK7 through an extensive network of interactions mediated by residues comprised within its putative α3, loop 1 and α4-loop 2 regions (Fig. 9, also Figs. 1 and 2), ultimately preventing binding of ATP and causing conformational changes that are incompatible with MKK7 catalytic function (Figs. 8 and 9, also Figs. 3 and 4).

Proposed Mechanism for Gadd45β-mediated Inhibition of MKK7—The final model, supported by extensive biochemical and site-directed mutagenesis data and molecular docking analyses, enables elaboration of a mechanism for Gadd45β-afforded inhibition of MKK7 (11). This model suggests that anchoring of Gadd45β to MKK7 is primarily mediated by electrostatic interactions and H-bonds formed between charged/polar residues positioned at the interface between the two proteins. Several contacts are seemingly established here between Lys^{149}, Lys^{157}, and Arg^{162} on the kinase active site and Glu^{65}, Glu^{66}, Glu^{113} on loops 1 and 2 of Gadd45β; further interactions appear to be established between Gln^{72} and Thr^{76} (α3) of Gadd45β and lysine residues within α3 of *MKK7* (Fig. 9*C*), and between residues within α4 and loop 2 (Gln^{96}, Gln^{109}, and Asp^{116}) of Gadd45β and β3 and the helix C-β3 loop of MKK7 (Arg^{152} and Arg^{153}). Finally, van der Waals interactions appear to be formed between Met^{95}/Gln^{96} (α4) of Gadd45β and Pro^{133}/Trp^{135} (β2) of MKK7, and between

Trp^{112}/Glu^{113} (loop 2) of Gadd45β and Thr^{190}/Asn^{189} (β4-β5 loop) of MKK7 (Fig. 9*C*). Analysis of the model also suggests that, during formation of the Gadd45β-MKK7 complex, interactions between Gadd45β and β2, β3, and helix C-β3 loop of MKK7 cause the β1 strand of the kinase to unfold and move away from the catalytic pocket, pushed by electrostatic repulsion by Gadd45β, it too being negatively charged (Figs. 7*A* and 9, *B* and *C*). This displacement of β1 would then enable insertion of acidic loop 1 into the catalytic pocket, where this could engage in H-bonds and polar interactions with Lys^{149} and other residues normally binding to the three-phosphate group of ATP (Fig. 9, *B* and *C*). Notably, this engagement of the ATP-binding site by loop 1 seems to prevent access of the kinase to ATP (11).

Notably, analysis of the three-dimensional models of MKK7 in its Gadd45β-bound and unbound states, raises the intriguing possibility that association with Gadd45β also causes the kinase to undergo conformational changes that further secure its inactivation. Indeed, as a result of interaction of α4-loop 2 of Gadd45β with β3 and the β3-helix C and β4-β5 loops of MKK7 and of occupancy of the catalytic pocket by loop 1, helix C of MKK7 appears to be pushed away from this pocket, to a position kinases normally have in their inactive conformation (Fig. 9*D*, see also Fig. 9*B*). Interestingly, however, the predicted overall conformation of Gadd45β-bound MKK7 is distinct from that seen in the typical, or "open," inactive conformation, because in the proposed model of the Gadd45β-MKK7 complex, the kinase activation loop retains its "active" position, that is away from the catalytic cleft, occupied in the complex by loop 1 (Fig. 9, *A* and *B*) (see also Refs. 27, 28, and 30). Yet, as seen in the typical open conformation, the key intramolecular bond between the invariant MKK7 residues, Lys^{149} (β3) and Asp^{166} (helix C), is disrupted by the interaction with Gadd45β (Fig. 9*D* and supplementary Figs. S4 and S5). Of interest, the aforementioned Gadd45β-induced conformational changes of MKK7 closely resemble those elicited on cyclin-dependent kinase 2 by its inhibitor $p27^{KIP1}$ (32). In keeping with the analogy with the proposed mechanism for Gadd45β-mediated blockade of MKK7, $p27^{KIP1}$ too targets the kinase ATP-binding site, preventing engagement of this site by ATP (32). Moreover, it too enters the catalytic pocket via displacement of strand β1 (32). It is noteworthy, however, that whereas the loop 1 of Gadd45β is predicted to contact residues in this pocket that interact with the three-phosphate group of ATP, $p27^{KIP1}$ engages residues of this pocket that normally accommodate the adenine ring of ATP (Fig. 9, *B* and *C*) (32).

Experimental Validation of the Model—This model for Gadd45β-mediated blockade of MKK7 is supported by compelling experimental evidence. It accounts for previous findings that region 132–156 of MKK7 (so-called peptide P1; comprising β2, β3, and the β3-helix C loop) is critical for anchoring to Gadd45β (supplementary Fig. S4). Consistently, soluble P1 effectively interferes with Gadd45β-mediated inhibition of MKK7, both *in vitro* and *in vivo* (11). The model also explains the ability of Gadd45β to block access of MKK7 to ATP, as well as the dispensability of MKK7 region 1–131 (comprising β1) for binding of the kinase to Gadd45β (Ref. 11, discussed above). Furthermore, both the model of MKK7 and Gadd45β were built on suitable structural templates, and robustness of both, as well as that of the model of the Gadd45β-MKK7 complex, was validated through extensive experimentation, including structural (Fig. 6 and supplementary Figs. S2 and S3; data not shown) and functional analyses (Figs. 1–4 and supplementary Fig. S5).

In vitro studies confirmed that region Ile^{69}–Asp^{86} (α3) is both required and sufficient for high affinity binding of Gadd45β to MKK7 (Figs. 1 and 2), and site-directed mutagenesis showed the importance of Gln^{72} and Thr^{76} within this region for this binding (Fig. 2, *D*, Mut-3; *B*, Ala-1 and Ala-2; see Fig. 9*C*). These data also supported a key role for α3 in docking of Gadd45β to MKK7 (*see* above). Moreover, they confirmed the model prediction that region Ile^{69}–Asp^{86} (α3) is insufficient alone to cause kinase inactivation (Fig. 4*B*, *69–86*), as this region contacts MKK7 at the outer brim of the catalytic pocket (Fig. 9, *B* and *C*). As also predicted by the model, Gadd45β inhibitory function requires at least one of two modules located within loop 1 and α4-loop 2 (Figs. 3 and 4). The key role of loop 1 in this function was shown by the finding that only peptide Ala^{60}–Asp^{86} (loop 1-α3), and not Ile^{69}–Asp^{86} (α3 alone), could afford blockade of MKK7, *in vitro* (Fig. 4*B*; also Fig. 3*D*, *1–86*). Consistently, this loop was also capable of stabilizing association of Gadd45β with MKK7, as mutation of Asp^{62}–Asp^{67} significantly weakened this association (Fig. 2*D*, *Mut-1*). Finally, the role of predicted salt bridge interactions between glutamic residues within putative loops 1 and 2 of Gadd45β (*i.e.* Glu^{65}, Glu^{66}, and Glu^{113}) and basic residues within the catalytic pocket of MKK7 (*i.e.* Lys^{149}, Lys^{157}, and Arg^{162}) were confirmed in GST pull-down assays performed with swapped protein mutants (supplementary Fig. 5).

The model also provides a basis for the observed inhibitory effects of loop 2 (Figs. 3, *B*, *69–160*; and 4, *B*, *69–113*). It shows in fact that by contacting the β3-helix C region of MKK7, this loop could cause conformational changes that impede catalytic function (Fig. 9, *A–D*). To cause these changes, however, loop 2 has to be positioned correctly in proximity of helix C, explaining why Gadd45β truncations lacking the docking module, α3, only have weak inhibitory effects despite the presence of α4-loop 2 (Fig. 3*B*, *87–160*; see also Fig. 9, *B* and *C*). In line with the ability of this α4-loop 2 region to interact with MKK7, Gadd45β proteins containing this region can bind, albeit weakly, to MKK7 even in the absence of α3 (Fig. 1*B*, *87–160*).

Finally, in addition to predicting residues contacting MKK7 (discussed above, Mut-1/Mut-3; Figs. 2, *C–D*, and 9*C*), the model confirms a role for others in maintenance of the global protein fold. It shows in fact that Gln^{79} and Asp^{86} (mutated in Mut-4 and Mut-5, respectively) could participate in intramolecular H-bonds that may stabilize the fold of Gadd45β (data not shown) and that Ile^{89}/Val^{90}/Val^{92} (mutated in Mut-6) are likely to be required for the secondary structure of β3 (Fig. 7*A*), which explains the marked binding impairment observed *in vitro* with Mut-4, Mut-5, and Mut-6 (Fig. 2*D*). Also, consistent with this view, is the finding that mutation of Gln^{79} and Asp^{86} appeared to have more dramatic effects in the context of Gadd45β(FL) than in that of Gadd45β-(60–86) (Fig. 2, *B* and *D*). The model finally illustrates how the partial binding defect

seen with Mut-7 is owed to involvement of Met^{95}/Gln^{96} in direct contact with MKK7 (Figs. 2*D* and 9*C*).

Relevance to Gadd45 Family Protein Functions and NF-κB—Gadd45 factors are emerging as a new class of kinase regulators, as they have been shown to modulate activity of various such enzymes, including Cdc2 and MAPK pathway kinases such as MEKK4, ASK1, MKK7, and p38 (11, 15, 17, 33–35). The kinase-binding region of these factors was previously delineated only for the Gadd45α-Cdc2 complex and was mapped to the highly conserved region of Gadd45α, Val^{69}–Glu^{84} (33), corresponding to the MKK7-binding module, α3, of Gadd45β (81.2% identity among the two regions; supplementary Fig. S6). Interestingly, the MKK7-binding regions of Gadd45β at loop 1 and α4-loop 2 are significantly less conserved among Gadd45 factors (supplementary Fig. S6), suggesting that, whereas α3 represents a common kinase-docking module, possibly explaining the promiscuity of these factors for kinase enzymes, the loop regions may account for specificity of the inhibitory action Gadd45 factors.

Additional conserved structures among Gadd45 proteins are the two dimerization modules. With Gadd45α, these modules were mapped to Gln^{33}–Ala^{61} and Ser^{132}–Arg^{165} (19), corresponding to Gln^{33}–Ile^{61} (β1-α2-β2) and Thr^{127}–Arg^{160} (β4/α5 loop-α5), respectively, of hGadd45β (supplementary Fig. S6). The high conservation of these regions suggests that they also mediate dimerization of Gadd45β. Yet, both appeared to be dispensable for Gadd45β-mediated binding and inactivation of MKK7 (Figs. 1–4). Consistent with this view, the dimerization surfaces of Gadd45β are well separated in space from those mediating contact with MKK7 (Fig. 7, *B* and *C*). Nevertheless, although monomeric Gadd45β retains strong inhibitory activity toward MKK7, *in vitro* (Fig. 4*B*, see *60–86*), it is possible that interaction of Gadd45β with MKK7, *in vivo*, occurs in the context of a heterotetrameric complex of the MKK7·Gadd45β:Gadd45β·MKK7 type. Hence, whereas it might play a role in association of Gadd45 factors with certain proteins (*e.g.* PCNA) (19), dimerization appears to have no immediate relevance to Gadd45β-mediated blockade of MKK7.

Altogether, these findings provide important new insights into the functions of Gadd45 proteins and the basis for NF-κB-mediated control of JNK signaling (2). Previously, we identified the Gadd45β-MKK7 interaction as a crucial molecular link between the NF-κB and JNK pathways (2, 11), and importance of this link was validated *in vivo* through the use of knock-out models and cell-permeable peptides that selectively disrupt its activity (2, 11). This importance, as well as the relevance of our model for Gadd45β-afforded blockade of MKK7 to the control of JNK signaling, *in vivo*, is further underscored by the finding that the regions of Gadd45β mediating suppression of MKK7, *in vitro* (*i.e.* loops 1 and 2 and helix α3; Figs. 3 and 4), are also responsible for blunting TNFα-induced killing, *in vivo* (Fig. 5). A note of caution is, however, warranted as the proposed model for Gadd45β-MKK7 interaction suffers from lack of "genuine" structural data, and so awaits final validation through x-ray crystallography studies. Notwithstanding, this model depicts the three-dimensional view that most accurately explains the wealth of experimental data and the results of the docking analyses presented in this study, affording a plausible detailed account of key molecular interactions between the two proteins.

These data further tighten the link between Gadd45β-mediated blockade of MKK7 and inhibition of PCD (2). Given the crucial role that the prosurvival activity of NF-κB plays in pathogenesis of widespread human diseases (see Refs. 1–3), these findings might help develop new therapies to treat these diseases.

REFERENCES

1. Kucharczak, J., Simmons, M. J., Fan, Y., and Gelinas, C. (2003) *Oncogene* **22,** 8961–8982
2. Papa, S., Bubici, C., Zazzeroni, F., Pham, C. G., Kuntzen, C., Knabb, J. R., Dean, K., and Franzoso, G. (2006) *Cell Death Differ.* **13,** 712–729
3. Karin, M. (2006) *Nature* **441,** 431–436
4. Claudio, E., Brown, K., and Siebenlist, U. (2006) *Cell Death Differ.* **13,** 697–701
5. Kim, H. J., Hawke, N., and Baldwin, A. S. (2006) *Cell Death Differ.* **13,** 738–747
6. De Smaele, E., Zazzeroni, F., Papa, S., Nguyen, D. U., Jin, R., Jones, J., Cong, R., and Franzoso, G. (2001) *Nature* **414,** 308–313
7. Tang, G., Minemoto, Y., Dibling, B., Purcell, N. H., Li, Z., Karin, M., and Lin, A. (2001) *Nature* **414,** 313–317
8. Davis, R. J. (2000) *Cell* **103,** 239–252
9. Deng, Y., Ren, X., Yang, L., Lin, Y., and Wu, X. (2003) *Cell* **115,** 61–70
10. Chang, L., Kamata, H., Solinas, G., Luo, J. L., Maeda, S., Venuprasad, K., Liu, Y. C., and Karin, M. (2006) *Cell* **124,** 601–613
11. Papa, S., Zazzeroni, F., Bubici, C., Jayawardena, S., Alvarez, K., Matsuda, S., Nguyen, D. U., Pham, C. G., Nelsbach, A. H., Melis, T., De Smaele, E., Tang, W. J., D'Adamio, L., and Franzoso, G. (2004) *Nat. Cell. Biol.* **6,** 146–153
12. Lu, B., Ferrandino, A. F., and Flavell, R. A. (2004) *Nat. Immunol.* **5,** 38–44
13. Gupta, M., Gupta, S. K., Balliet, A. G., Hollander, M. C., Fornace, A. J., Hoffman, B., and Liebermann, D. A. (2005) *Oncogene* **24,** 7170–7179
14. Ijiri, K., Zerbini, L. F., Peng, H., Correa, R. G., Lu, B., Walsh, N., Zhao, Y., Taniguchi, N., Huang, X. L., Otu, H., Wang, H., Fei Wang, J., Komiya, S., Ducy, P., Rahman, M. U., Flavell, R. A., Libermann, T. A., and Goldring, M. B. (2005) *J. Biol. Chem.* **280,** 38544–38555
15. Takekawa, M., and Saito, H. (1998) *Cell* **95,** 521–530
16. Liebermann, D. A., and Hoffmann, B. (2002) *Oncogene* **21,** 3391–3402
17. Papa, S., Zazzeroni, F., Pham, C. G., Bubici, C., and Franzoso, G. (2004) *J. Cell Sci.* **117,** 5197–5208
18. Snyder, E. L., and Dowdy, S. F. (2001) *Curr. Opin Mol. Ther.* **3,** 147–152
19. Kovalsky, O., Lung, F. D., Roller, P. P., and Fornace, A. J., Jr. (2001) *J. Biol. Chem.* **276,** 39330–39339
20. Yang, J. T., Wu, C. S., and Martinez, H. M. (1986) *Methods Enzymol.* **130,** 208–269
21. D'Ambrosio, C., Talamo, F., Vitale, R. M., Amodeo, P., Tell, G., Ferrara, L., and Scaloni, A. (2003) *Biochemistry* **42,** 4430–4443
22. Shi, J., Blundell, J., and Mizuguchi, K. (2001) *J. Mol. Biol.* **310,** 243–257
23. Marchler-Bauer, A., and Bryant, S. H. (2004) *Nucleic Acids Res.* **32,** 327–331
24. Koonin, E. V. (1997) *J. Mol. Med.* **75,** 236–238
25. Vidovic, I., Nottrott, S., Hartmuth, K., Lührmann, R., and Ficner, R. (2000) *Mol. Cell* **6,** 1331–1342
26. Schultz, A., Nottrott, S., Watkins, N. J., and Luhrmann, R. (2006) *Mol. Cell. Biol.* **26,** 5146–5154
27. Hanks, S., and Hunter, T. (1995) *FASEB J.* **9,** 576–596
28. Hubbard, S. R. (1997) *EMBO J.* **16,** 5572–5581
29. Zhou, T., Raman, M., Gao, Y., Earnest, S., Chen, Z., Machius, M., Cobb, M. H., and Goldsmith, E. J. (2004) *Structure* **12,** 1891–1900
30. Ohren, J. F., Chen, H., Pavlovsky, A., Whitehead, C., Zhang, E., Kuffa, P., Yan, C., McConnell, P., Spessard, C., Banotai, C., Mueller, W. T., Delaney, A., Omer, C., Sebolt-Leopold, J., Dudley, D. T., Leung, I. K., Flamme, C.,

Warmus, J., Kaufman, M., Barrett, S., Tecle, H., and Hasemann, C. A. (2004) *Nat. Struct. Mol. Biol.* **11,** 1192–1197
31. Chen, R., Li, L., and Weng, Z. (2003) *Proteins* **52,** 80 – 87
32. Russo, A. A., Jeffrey, P. D., Patten, A. K., Massague, J., and Pavletich, N. P. (1996) *Nature* **382,** 325–331
33. Jin, S., Antinore, M. J., Lung, F. D., Dong, X., Zhao, H., Fan, F., Colchagie, A. B., Blanck, P., Roller, P. P., Fornace, A. J., Jr., and Zhan, Q. (2000) *J. Biol. Chem.* **275,** 16602–16608
34. Bulavin, D. V., Kovalsky, O., Hollander, M. C., and Fornace, A. J., Jr. (2003) *Mol. Cell. Biol.* **23,** 3859 –3871
35. Salvador, J. M., Mittelstadt, P. R., Belova, G. I., Fornace, A. J., Jr., and Ashwell, J. D. (2005) *Nat. Immunol.* **6,** 396 – 402